JACS
JOURNAL OF THE AMERICAN CHEMICAL SOCIETY
Article
pubs.acs.org/JACS

Cocrystals of Nicotinamide and (*R*)-Mandelic Acid in Many Ratios with Anomalous Formation Properties

Si-Wei Zhang, Michelle T. Harasimowicz, Melgardt M. de Villiers, and Lian Yu*

School of Pharmacy and Department of Chemistry, University of Wisconsin-Madison, Madison, Wisconsin 53705, United States

Supporting Information

ABSTRACT: We report a remarkable system of cocrystals containing nicotinamide (NIC) and (*R*)-mandelic acid (RMA) in numerous stoichiometric ratios (4:1, 1:1 in two polymorphs, and 1:2) with anomalous formation properties. The formation of these cocrystals decreases energy but expands volume, in contrast to most physical processes, but similar to water freezing. The decrease of energy upon cocrystallization agrees with the exothermic mixing of NIC and RMA liquids (a base and an acid). Volume expansion is general for the formation of all NIC cocrystals for which data exist (n = 40): +3.9 Å^3/molecule or +17 cm^3/kg on average, corresponding to a 2% expansion. This volume expansion correlates with the shortening and strengthening of hydrogen bonds upon cocrystallization, analogous to water freezing. The NIC-RMA binary phase diagram was constructed that contains the congruent and incongruent melting of six crystalline phases. These results are relevant for understanding the nature of cocrystallization and why some molecules are prolific cocrystal formers.

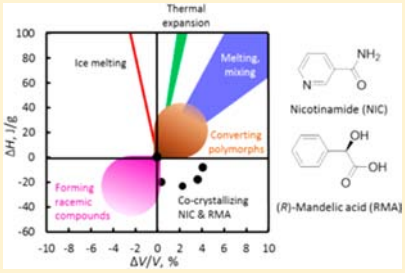

INTRODUCTION

The ability of different chemical components to cocrystallize in the same lattice is an important phenomenon in science and technology. Cocrystals have been known for a long time, under the name "compound" for a fixed component ratio, and "solid solution" for variable stoichiometry.[1] Interest in organic cocrystals has grown in recent years, driven in part by their applications in engineering pharmaceutical solids[2−5] and other molecular materials.[6] Despite many studies, however, the nature of cocrystallization remains inadequately understood. The complexity of organic molecules—irregular shape, chirality, flexibility, and hydrogen bonding—makes their cocrystallization fundamentally different from that of metals and other inorganic substances. It remains a mystery why some molecules (e.g., nicotinamide[7−10]) are prolific cocrystal formers. There have been systematic studies on racemic compounds, a special class of cocrystals containing opposite enantiomers,[11,12] but it is unclear whether the conclusions apply to other cocrystals; for example, whether cocrystallization simultaneously lowers energy and reduces volume. Answering these questions helps advance the science of cocrystallization to technological benefit.

We report an extraordinary system of cocrystals containing nicotinamide (NIC) and (*R*)-mandelic acid (RMA, Scheme 1) in many stoichiometric ratios (4:1, 1:1 in two polymorphs, and 1:2). This abundance of structures helps elucidate the nature of cocrystallization, much like the availability of many polymorphs aids in the study of structure−property relations.[13] The NIC-RMA cocrystals are remarkable in that their formation from the component crystals lowers energy but expands volume, which stands in contrast to the positive energy−volume correlation in most physical processes. A survey of all NIC cocrystals found that they generally have positive formation volumes (+3.9 Å^3/molecule or +17 cm^3/kg on average) and contain shorter and stronger hydrogen bonds. In this respect, the formation of NIC cocrystals is analogous to water freezing, which also features a negative enthalpy−volume correlation. These results are relevant for understanding the formation of organic cocrystals and why NIC is a prolific coformer.

Scheme 1. Structures of Nicotinamide (NIC) and (*R*)-Mandelic Acid (RMA)[a]

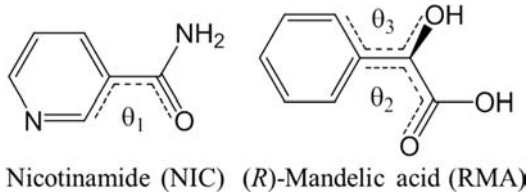

Nicotinamide (NIC) (*R*)-Mandelic acid (RMA)

[a] θ_1, θ_2, and θ_3 indicate angles of torsion.

METHODS

(*R*)-Mandelic acid (RMA) and nicotinamide (NIC; the stable polymorph[14]) were purchased from Sigma-Aldrich (St. Louis, MO, USA) and used as received. Acetonitrile (HPLC grade) and chloroform (ACS reagent grade) were purchased from Fisher Scientific (Pittsburgh, PA, USA).

Powder X-ray diffraction was performed with a Bruker D8 Advance diffractometer (Cu Kα radiation, voltage 40 kV, and current 40 mA). Approximately 5 mg of powder was sprinkled on the surface of a zero-background silicon (510) sample holder and scanned from 2 to 40° 2θ at a speed of 1.2°/min and a step size of 0.02°. Single-crystal X-ray diffraction evaluation and data collection were performed at 100 K on a Bruker SMART APEXII diffractometer with Cu Kα radiation, and the crystal structure was solved using a standard procedure (see the

Received: October 14, 2013
Published: November 11, 2013

   dx.doi.org/10.1021/ja4103887 | *J. Am. Chem. Soc.* 2013, 135, 18981−18989

Table 1. Structures of NIC and RMA Crystals and NIC-RMA Cocrystals

	RMA	NR_2	NR Form 1 (JILZOU)	NR Form 2 (JILZOU01)	N_4R	NIC (NICOAM02)
T, K	100(1)	100(1)	150(2)	100(1)	100(1)	295
wavelength, Å	1.54178	1.54178	0.71073	1.54178	1.54178	0.71073
cryst system	monoclinic	triclinic	monoclinic	monoclinic	monoclinic	monoclinic
space group	$P2_1$	$P1$	$C2$	$P2_1$	$P2_1$	$P2_1/c$
cryst size, mm^3	0.24 × 0.22 × 0.03	0.35 × 0.18 × 0.07	0.46 × 0.07 × 0.07	0.28 × 0.18 × 0.16	0.20 × 0.10 × 0.10	0.8 × 0.7 × 0.6
a, Å	8.377(4)	6.5020(12)	32.6557(9)	5.2406(3)	6.0810(7)	3.975(5)
b, Å	5.859(2)	7.5220(8)	5.475(1)	10.0477(6)	34.245(4)	15.632(8)
c, Å	15.047(5)	20.6532(17)	14.9264(5)	12.6006(7)	7.4405(9)	9.422(4)
α, deg	90	97.770(5)	90	90	90	90
β, deg	103.08(2)	91.964(4)	99.400(1)	95.678(4)	99.280(9)	99.03(7)
γ, deg	90	90.557(5)	90	90	90	90
V, $Å^3$	719.4(5)	1000.1(2)	2632.9(5)	660.24(7)	1529.2(3)	578.2
Z	2	2	8	2	2	4
ρ_{calcd}, g cm^{-3}	1.405	1.416	1.384	1.380	1.391	1.403
μ, mm^{-1}	0.910	0.893	0.103	0.857	0.838	0.1
$F(000)$	320.0	448	1152	288	672	*a*
θ range, deg	3.015−72.267	2.16−72.437	3.77−27.43	3.52−67.60	2.58−71.24	8.14−13.46
no. of data/restraints/params	2773/1/216	7540/3/608	5773/1/361	1235/1/183	5726/1/465	*a*
S	1.046	1.038	1.12	1.011	1.070	0.040
R_1, wR_2 ($I > 2\sigma(I)$)	0.0284, 0.0768	0.0270, 0.0746	0.055, 0.128	0.0430, 0.1138	0.0472, 0.1151	0.057, 0.066
R_1, wR_2 (all data)	0.0314, 0.0802	0.0281, 0.0762	0.070, 0.138	0.0472, 0.1174	0.0542, 0.1190	*a*
min, max Δ, e $Å^{-3}$	−0.16, 0.22	−0.14, 0.24	−0.295, 0.293	−0.248, 0.306	−0.208, 0.208	−0.182, 0.490

[a]Original data not found.

Supporting Information for details). Raman microscopy was performed with a Thermo Scientific DXR Raman microscope and a 10 mW 532 nm laser and was used to distinguish crystal polymorphs. Differential scanning calorimetry (DSC) was conducted with a TA Instruments Q2000 unit under 50 mL/min N_2 purge, with a sample typically 5−10 mg in a crimped or Tzero aluminum pan. In a typical run, the sample was heated at 5 or 10 °C/min to 160 °C to measure the temperature and heat of melting, cooled at 10 °C/min, and heated again at 10 °C/min to record the glass transition temperature of the melt. Hot-stage microscopy was performed with a Linkam THMS 600 hot stage and an Olympus BH2-UMA light microscope.

Seeds of cocrystals were obtained by melt crystallization and used later for growing higher-quality crystals from solution.[10] In a typical experiment, a melt of a chosen NIC:RMA ratio was formed between two coverslips and allowed to crystallize at room temperature, and the resulting crystals were analyzed by X-ray diffraction for new crystalline phases. For seeded crystallization, a filtered acetonitrile solution of NIC (0.5 M) and RMA (0.125 M) was used to crystallize the 4:1 NIC-RMA cocrystal, and a chloroform solution of NIC (0.25 M) and RMA (0.5 M) was used to crystallize the 1:2 NIC-RMA cocrystal. The solutions were filtered and seeded at room temperature.

To prepare a physical mixture of NIC and RMA crystals, each material was passed through a sieve with 250 μm openings. The sieved powders were mixed at desired ratios with a vortex mixer (Vortex Genie K-550-G Mixer) at the maximum speed for 1 min. The final mixture was analyzed by X-ray diffraction to ensure that it contained only component crystals and no cocrystals, and was used immediately for subsequent DSC analysis.

The formation property of a cocrystal A_mB_n is defined in reference to eq 1:

$$mA + nB \rightarrow A_mB_n \quad (1)$$

where A and B are the crystal of component A (NIC) and the crystal of component B (RMA), respectively. Equation 2 is used to determine the formation enthalpy:

$$\Delta H_f = \Delta H_{m(A+B)}(T_S \rightarrow T_L) - \Delta H_{mAB}(T_S \rightarrow T_L) \quad (2)$$

where T_S is a temperature at which the cocrystal and the physical mixture of component crystals are solid and at which ΔH_f is evaluated, T_L is a temperature at which the cocrystal and the physical mixture are both melted to the same liquid, and $\Delta H_{m(A+B)}$ ($T_S \rightarrow T_L$) and ΔH_{mAB} ($T_S \rightarrow T_L$) are the corresponding enthalpies of melting (properly scaled to reflect the stoichiometry of the cocrystal).

The mixing enthalpy of a liquid of NIC and a liquid of RMA is determined by eq 3:

$$\Delta H_{mix} = \Delta H_{m(A+B)}(T_S \rightarrow T_L) - \Delta H_{mA}(T_S \rightarrow T_L) - \Delta H_{mB}(T_S \rightarrow T_L) \quad (3)$$

where T_S is a temperature at which NIC, RMA, and their physical mixture are all solids, T_L is a temperature at which the three materials are all melted and at which ΔH_{mix} is evaluated, and ΔH_{mA} ($T_S \rightarrow T_L$), ΔH_{mB} ($T_S \rightarrow T_L$) and $\Delta H_{m(A+B)}$ ($T_S \rightarrow T_L$) are the corresponding enthalpies of melting (properly scaled to reflect the solution composition).

RESULTS AND DISCUSSION

Discovery of NIC-RMA Cocrystals of Different Stoichiometries and Their Structures. The cocrystallization of NIC and RMA produces a remarkable number of structures of different stoichiometries. In addition to the 1:1 cocrystal of Friščić and Jones,[7] work in this laboratory has discovered three more: a new polymorph of the 1:1 cocrystal,[10] a 4:1 cocrystal, and a 1:2 cocrystal. For convenience, we shall refer to these cocrystals as NR Form 1, NR Form 2, N_4R, and NR_2. Our search for new cocrystals relied on melt crystallization to obtain crystal seeds.[15] Melts of NIC and RMA at different ratios were crystallized and the products analyzed by X-ray diffraction for new phases; Figures S1 and S2 in the Supporting Information illustrate the data collected for this purpose. We obtained seeds of NR Form 1 and NR Form 2 by crystallizing a 1:1 melt[10] and seeds of N_4R by crystallizing a 4:1 melt. (There is some evidence that the formation of N_4R involved a solid-state transformation from a metastable phase.) Unexpectedly, seeds of NR_2 crystallized from a 1:4 melt. We attempted to crystallize NR_2 congruently from a 1:2 melt, but the melt crystallized much more slowly.

dx.doi.org/10.1021/ja4103887 | J. Am. Chem. Soc. 2013, 135, 18981−18989

Table 2. Torsional Angles of the NIC and RMA Crystals and NIC-RMA Cocrystals

NIC conformation					
	NR Form 1	NR Form 2	N_4R	NR_2	pure NIC[a]
θ_1, °	35.3 (mol.1) 12.0 (mol.2)	-28.8	-162.6 (mol.1), 162.8 (mol.2) -167.1 (mol.3), 164.2 (mol.4)	-17.7 (mol.1), -20.1 (mol.2)	-157.4
RMA conformation					
	NR Form 1	NR Form 2	N_4R	NR_2	pure RMA[b]
θ_2, °	-103.3 (mol.1) -129.5 (mol.2)	-106.0	-101.4	-126.5 (mol.1), 59.4 (mol.2) -124.8 (mol.3), 59.3 (mol.4)	-122.0 (mol.1) -124.5 (mol.2)
θ_3, °	138.0 (mol.1) 135.1 (mol.2)	104.8	109.0	100.4 (mol.1), 87.3 (mol.2) 140.9 (mol.3), 143.1 (mol.4)	150.3 (mol.1) 96.5 (mol.2)

[a]Retrieved from CSD (NICOAM02). θ_1 is defined in Scheme 1. [b]The values of θ_2 and θ_3 for RMA are from this work and are slightly different from those given in ref 10, which were obtained from the structure of SMA by symmetry. θ_2 and θ_3 are defined in Scheme 1.

With seeds obtained from melt crystallization, solution crystallization was performed to produce crystals of higher quality for structural solution and other analyses. Table 1 shows the structural parameters of NIC-RMA cocrystals and their component crystals.[7,10,16] Table 2 compares the molecular conformations of NIC and RMA in these crystals. For NIC, conformational flexibility is associated mainly with the amide torsion relative to the pyridine ring (θ_1 in Scheme 1). In the pure NIC crystal, NIC has a conformation in which the amide O is on the opposite side of the pyridine N (θ_1 approaching 180°). This conformation is close to the global minimum of conformational energy relative to θ_1.[8] NIC adopts a similar conformation in N_4R but different conformations in the other cocrystals, with θ_1 being rotated ca. 180°, close to a local minimum 4 kJ/mol above the global minimum. Conformational differences are also seen in the RMA molecule; see torsional angles θ_2 and θ_3 defined in Scheme 1 and tabulated in Table 2. Note especially that two of the four RMA molecules in NR_2 have conformations substantially different from those in pure RMA and the other cocrystals.

Figure 1 shows the different networks of hydrogen bonds in the cocrystals. In NR Form 1, NIC molecules form amide−amide $R_2^2(8)$ "homo-dimers", to which RMA molecules are bonded (carboxylic acid to the pyridine N). In NR Form 2, NIC and RMA molecules form $R_2^2(9)$ "hetero-dimers" through the amide and the α-hydroxyl carbonyl group; these hetero-dimers are further joined by hydrogen bonds to form ribbons along b.[10] In N_4R, NIC molecules also form amide−amide $R_2^2(8)$ homo-dimers as in NR Form 1; these homo-dimers join by hydrogen bonds to form ribbons along [101]. The ribbons further join by hydrogen bonding with RMA molecules. In NR_2, NIC and RMA molecules form $R_2^2(8)$ hetero-dimers (amide to carboxylic acid), which further join to form ribbons along [110]; the ribbons are connected by hydrogen bonds with RMA molecules (carboxylic acid to pyridine N).

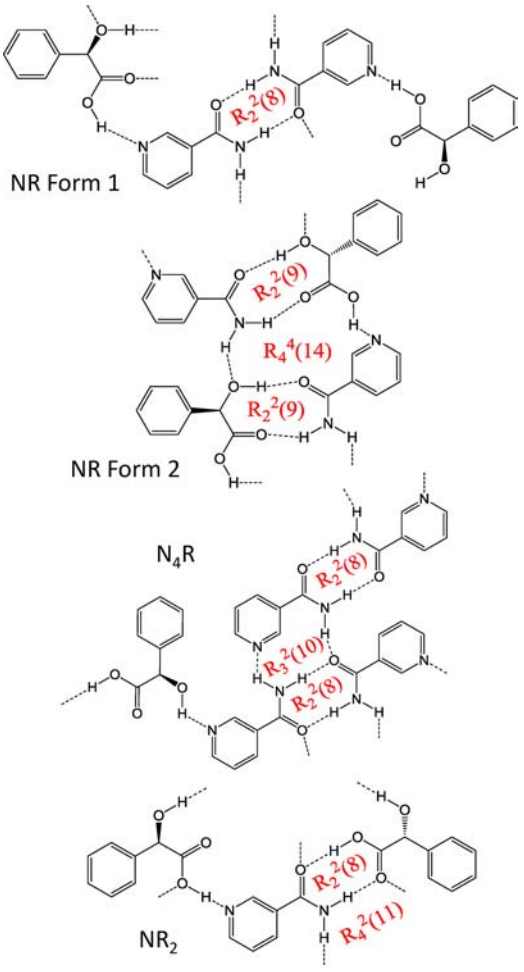

Figure 1. Hydrogen bonds in NIC-RMA cocrystals.

Volume Expansion upon Cocrystallization. A remarkable property of NIC-RMA cocrystals is their looser molecular packing relative to the component crystals. We demonstrate this conclusion with the data in Figure 2. Figure 2a shows the volume of one molecule in the crystals of NIC and RMA and in their cocrystals, all calculated from crystallographic data using $V = V_{cell}/Z$, where V_{cell} is the volume of the unit cell and Z the number of molecules therein. One "molecule" in a cocrystal A_mB_n consists of $m/(m+n)$ of A and $n/(m+n)$ of B. The V thus obtained is the volume occupied by one molecule in a crystal *including void space*. For NIC and RMA, V is known at different temperatures (NIC at 150 K (CSD Refcode NICOAM01) and 295 K (NICOAM02, 03);[16] RMA at 295 K (FEGHAA)[17] and 100 K (this work)), yielding a thermal expansion coefficient α_V of 2.1×10^{-4} K^{-1} for both systems ($\alpha_V = d(\ln V)/dT$). This α_V value is typical for organic solids and allows the calculation of V at different temperatures.

Figure 2b shows the molecular volumes at 100 K in the crystals of NIC and RMA and their cocrystals. Most are experimental data determined at 100 K; the value for NIC is obtained by extrapolating the data at 150 and 295 K (Figure 2a), and the value for NR Form 1 is obtained from the data at 150 K and $\alpha_V = 2.1 \times 10^{-4}$ K^{-1}. Given that NIC and RMA have identical α_V values, we assume the values for their cocrystals to be similar. Figure 2b shows that that every NIC-RMA cocrystal has a molecular

dx.doi.org/10.1021/ja4103887 | J. Am. Chem. Soc. 2013, 135, 18981−18989

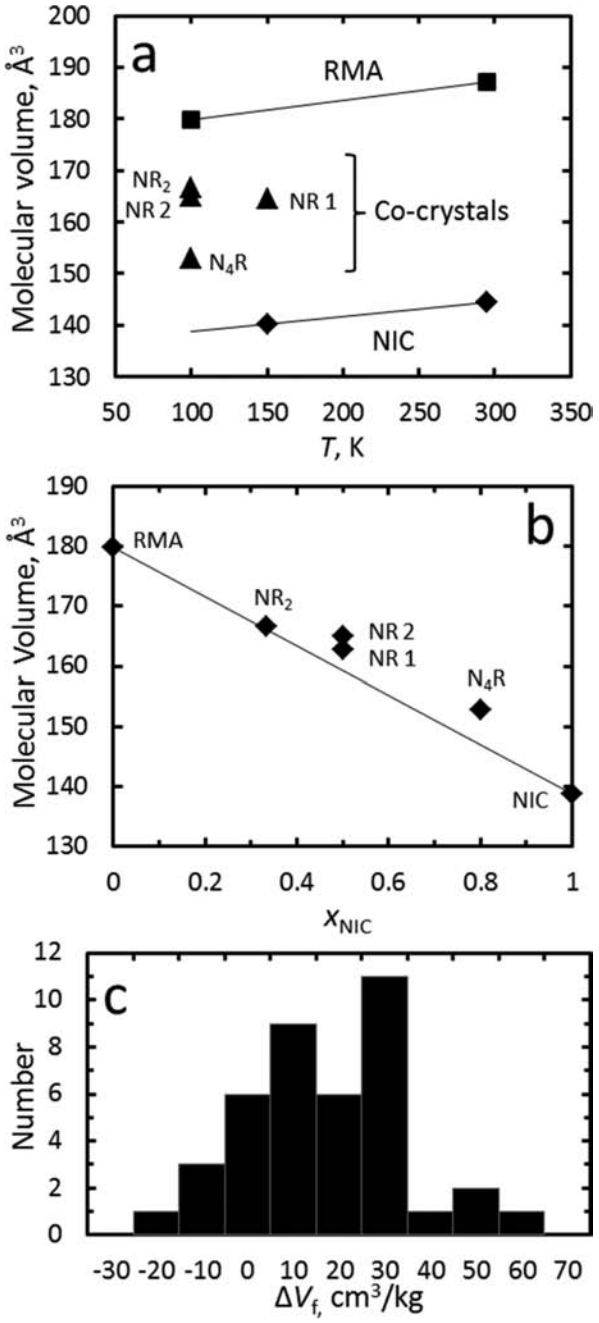

Figure 2. Molecular volumes in the crystals of NIC and RMA and in their cocrystals plotted against temperature (a) and at 100 K (b). The lines in (a) correspond to $\alpha_V = 2.1 \times 10^{-4}$ K^{-1}. (c) Formation volumes ΔV_f of all NIC-containing cocrystals in the CSD (n = 40).

volume larger than the weighted average of the values of the component crystals (the line). In other words, the cocrystals have positive volumes of formation, defined as

$$\Delta V_f = V_{cc} - [m/(m+n)V_A + n/(m+n)V_B] \quad (4)$$

In Figure 2b, ΔV_f is the vertical distance from a cocrystal point to the line between NIC and RMA: ΔV_f (Å^3/molecule) = +0.5 (NR_2), +3.6 (NR Form 1), +5.8 (NR Form 2), and +5.9 (N_4R). In cm^3/kg, we find ΔV_f (cm^3/kg) = +2.3 (NR_2), +15.6 (NR Form 1), +25.3 (NR Form 2), and +28.0 (N_4R). Though evaluated at 100 K, these values are expected to be insensitive to temperature, given the similar thermal expansion coefficients of NIC and RMA.

The positive formation volumes of the NIC-RMA cocrystals are surprising because, as we discuss below, they have *negative* enthalpies of formation. Furthermore, the mixing of acids and bases in the liquid state is known to *reduce* volume.[18] To test the generality of our observation, we examined all cocrystals containing NIC in the CSD[19] under the following constraints: 3D atomic coordinates determined, $R \leq 0.1$, no errors, not polymeric, no ions, and organics only. Structures solved from powder patterns were excluded, as well as those of clathrates, solvates, and cocrystals with more than two components. The remaining hits are given in Table 3, along with the data on component B (coformer), retrieved with the same criteria. Table 3 and Figure 2c show that most cocrystals containing NIC (34 of 40) have positive ΔV_f values, with an average value of +3.9 Å^3/molecule and +17 cm^3/kg. These values are similar to those for the subgroup containing NIC and RMA, suggesting the subgroup well represents the entire set of NIC cocrystals. These data indicate that, in all NIC cocrystals, the average molecule occupies a volume 2% larger than that in the individual component crystals. There is no significant dependence of ΔV_f on the temperature at which it is evaluated, which is consistent with the similar thermal expansion coefficients of the crystals. Note that the molecules crystallizing with NIC have different sizes: V_B ranges from 30% smaller than V_{NIC} to 3 times larger; on average, V_B is slightly larger than V_{NIC} (218 Å^3 vs 140 Å^3). Despite the different sizes of the coformers, however, there is no significant dependence of ΔV_f on V_B. This insensitivity suggests that the volume expansion upon cocrystallization is not a simple consequence of packing molecules of different sizes. We will later argue that the expansion reflects the formation of more open structures containing stronger hydrogen bonds.

van de Streek and Motherwell compared the molecular volumes in hydrated and anhydrous crystals and concluded that a molecule tends to occupy a larger volume (by 1.2%) upon cocrystallizing with water.[20] In their analysis, the volume of water V_w is given a value estimated from the average atomic volumes in organic crystals, which does not reflect water−water hydrogen bonding. Their analysis would be formally equivalent to ours if V_w were calculated from the density of ice, which would need to be extrapolated to 298 K, the temperature of their analysis. Doing so would increase the V_w value and decrease the 1.2% value for the expansion of molecular volume upon hydrate formation. Price et al. compared the packing efficiencies of solvated and solvent-free crystals.[21] For several prolific solvate-forming molecules, they reported that space is more or less efficiently filled in solvated crystals than in solvent-free crystals. Their study differs from ours in that the pure solvent phase is not included in the reference state (roughly equivalent to our comparing a cocrystal's packing efficiency with that of only one component crystal). It is also worth noting that our analysis is based entirely on experimental densities obtained from crystal structures (Table 3), whereas previous studies make model-dependent assumptions about molecular volumes; for example, van der Waals volumes are used for calculating packing efficiencies.[21] It would be valuable to apply a consistent analysis to various systems of interest to understand the nature of molecular packing in single- and multiple-component crystals.

Thermodynamics of NIC-RMA Cocrystals. Figure 3 shows the DSC traces of NIC-RMA cocrystals and the component crystals. NR Form 1 and Form 2 melt congruently; N_4R and NR_2 melt incongruently. Cooling a melt of NIC and RMA could

dx.doi.org/10.1021/ja4103887 | J. Am. Chem. Soc. 2013, 135, 18981−18989

Table 3. Formation Volumes ΔV_f of Cocrystals Containing Nicotinamide (NIC)[a]

coformer B	cocrystal refcode	*m*	*n* (B)	M_{cc}, g/mol	T_{cc}, K	V_{cc}, Å^3	V_{NIC}, Å^3	V_B, Å^3	α_{VB}, 10^{-4}K^{-1}	coformer refcode	ΔV_f, Å^3	ΔV_f, cm^3/kg
3-hydroxy-2-naphthoic acid	ABULEQ	1	1	155.15	293	180.099	144.490	227.783	n.a.	HNAPAC	-6.0	-23.4
citric acid	CUYXUQ	2	1	145.45	293	161.393	144.490	192.736	1.7	CITRAC10, 11	0.8	3.4
succinic acid	DUZPAQ	2	1	120.78	120	136.335	139.333	120.609	2.0	SUCACB08, 09	3.2	16.2
5-methyl benzene-1,3-diol	EWAQAV	4	1	122.52	150	146.429	140.214	161.540	n.a.	EWAMAR	1.9	9.6
flufenamic acid	EXAQAW	1	1	201.68	100	225.295	138.749	304.803	n.a.	FPAMCA17	3.5	10.5
margaric acid	FIFLAI	1	1	196.29	293	289.032	144.490	441.600	n.a.	DARWAU	-4.0	-12.3
baicalein	GAZWUB	1	1	196.18	100	217.918	138.749	291.789	2.0	RAMGOB01	2.6	8.1
ethyl paraben	GOGQID	1	1	144.15	113	171.836	139.128	206.129	n.a.	FEGLEI	-0.8	-3.3
indole-3-acetic acid	IACNCA	1	1	148.65	295	181.886	144.550	216.835	1.6	INACET01, 02	1.2	4.8
palmitic acid	JEMDIP	1	1	189.27	298	285.462	144.641	414.493	n.a.	YEFWEM	5.9	18.8
(*R*)-mandelic acid	JILZOU	1	1	137.14	150	164.557	140.214	181.712	2.1	FEGHAA, this work	3.6	15.8
(*R*)-mandelic acid	JILZOU01	1	1	137.14	100	165.061	138.749	179.840	2.1	this work	5.8	25.3
(*R*)-mandelic acid	N_4R	4	1	128.13	100	152.916	138.749	179.840	2.1	this work	5.9	28.0
(*R*)-mandelic acid	NR_2	1	2	142.14	100	166.690	138.749	179.840	2.1	this work	0.5	2.3
malonic acid	NUKXUN	2	1	116.10	180	135.932	141.100	104.351	1.8	MALNAC02,04-6,09	7.1	36.7
fumaric acid	NUKYAU01	1	1	119.10	293	137.156	144.490	118.189	n.a.	FUMAAC	5.8	29.4
fumaric acid	EDAPOQ	2	1	120.10	295	146.588	144.550	118.189	n.a.	FUMAAC	10.8	54.3
glutaric acid	NUKYEY	1	1	127.12	180	144.488	141.100	150.381	3.2	GLURAC, 02-4	-1.3	-5.9
adipic acid	NUKYIC	1	1	134.13	180	160.178	141.100	174.365	2.2	ADIPAC,03,08,09,13	2.4	11.0
adipic acid	NUKYOI	2	1	130.13	180	154.163	141.100	174.365	2.2	ADIPAC,03,08,09,13	2.0	9.1
pimelic acid	NUKYUO01	1	1	141.15	110	168.928	139.041	192.743	2.8	PIMELA07	3.0	13.0
pimelic acid	NUKYUO02	1	1	141.15	110	179.541	139.041	192.743	2.8	PIMELA07	13.6	58.2
suberic acid	NUKZAV	1	1	148.16	180	189.825	141.100	222.108	1.8	SUBRAC01, 05	8.2	33.4
suberic acid	NUKZEZ	2	1	139.48	180	170.151	141.100	222.108	1.8	SUBRAC01, 05	2.0	8.8
azelaic acid	NUKZID	1	1	155.17	180	205.588	141.100	242.860	2.2	AZELAC03	13.6	52.8
sebacic acid	NUKZOJ	2	1	148.83	180	186.510	141.100	271.122	2.1	SEBAAC03	2.1	8.4
4-hydroxy-3-methoxybenzaldehyde	OBUBOE	1	1	137.14	100	159.380	138.749	181.501	1.6	YUHTEA, 01, 03	-0.7	-3.3
octadecanoic acid	PEQBES	1	1	203.30	295	308.027	144.550	452.469	n.a.	STARAC02	9.5	28.2
4-hydroxy benzoic acid	RUYHEZ01	1	1	130.12	293	152.429	144.490	153.171	n.a.	JOZZIH	3.6	16.7
(*RS*)-ibuprofen	SODDIZ	1	1	164.21	120	224.560	139.333	292.879	2.5	IBPRAC, 01, 02	8.5	31.0
salicylic acid	SODDOF	1	1	130.12	120	155.020	139.333	155.658	1.2	SALIAC17	7.5	34.8
(*S*)-ibuprofen	SOGLAC	1	1	164.21	120	224.909	139.333	300.057	2.3	JEKNOC, 10, 12	5.2	19.1
2-chloro-4-nitrobenzoic acid	SUTTUX	1	1	161.84	293	176.106	144.490	201.756	n.a.	VOLZEC01	3.0	11.1
lauric acid	UCOTUC	1	1	161.22	298	238.606	144.641	319.095	n.a.	LAURAC01	6.7	25.2
isonicotinamide	UMUYOR	1	1	122.12	100	148.087	138.749	147.125	n.a.	EHOWIH04	5.2	25.4
carbamazepine	UNEZES	1	1	179.20	200	220.180	141.694	287.575	1.9	Ref. 22	5.5	18.6
3-hydroxy benzoic acid	XAQQIQ	1	1	130.12	100	150.364	138.749	150.136	n.a.	BIDLOP, 01	5.9	27.4
benzene-1,2,3-triol	HEDROZ	1	2	124.78	100	136.939	138.749	135.631	n.a.	PYRGAL02	0.3	1.3
(*S*)-naproxen	HEGGAD	1	2	194.21	223	244.643	142.381	300.570	1.6	COYRUD, 11, 12	-3.2	-9.9
2,5-dihydroxy benzoic acid	PEKRUU	1	1	138.12	295	159.272	144.550	162.099	1.3	BESKAL, 08	5.9	25.9

[a] *m* and *n* describe the stoichiometry of cocrystal A_mB_n (A = NIC, B = coformer). *M*: molecular weight (cc = cocrystal); T_{cc}: temperature at which cocrystal structure is determined and ΔV_f is evaluated. *V*: molecular volume at T_{cc}. α_{VB}: thermal expansion coefficient of B. If necessary, V_{NIC} is temperature-corrected with $\alpha_V = 2.1\times10^{-4}$ K^{-1}. Temperature-correction of V_B is made if $|T_B - T_{cc}| > 5$ K. If the B structure is known at several temperatures, α_{VB} is calcd. (shown) and used for correcting V_B; otherwise (flagged "n.a."), α_{VB} is assumed to be 2×10^{-4} K^{-1}. If B is polymorphic, densest polymorph at evaluation temperature is chosen. Error in ΔV_f is 0.5 Å^3 or 2 cm^3/kg.

dx.doi.org/10.1021/ja4103887 | J. Am. Chem. Soc. 2013, 135, 18981−18989

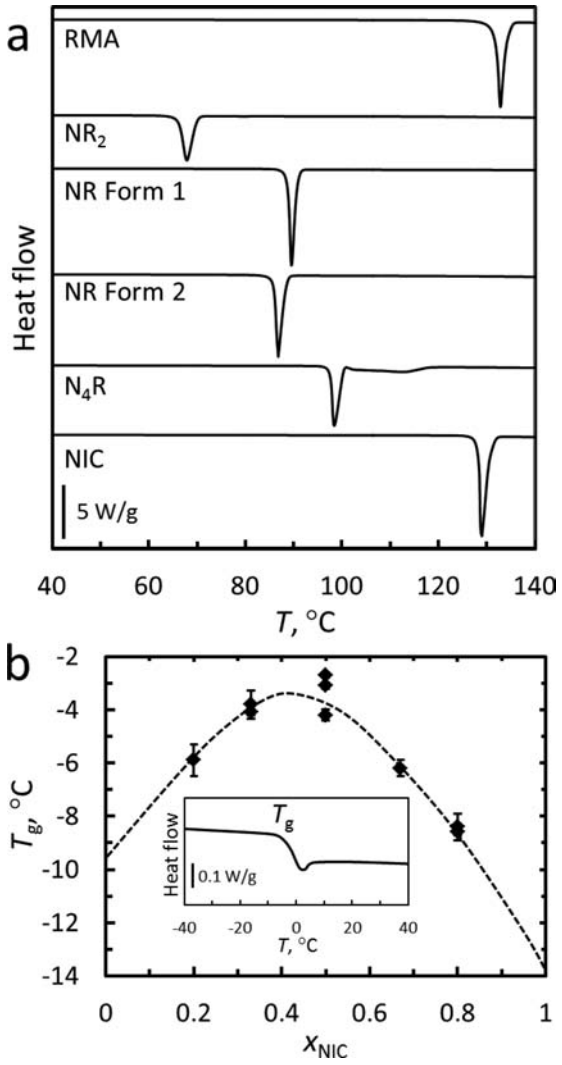

Figure 3. (a) DSC melting traces of NIC, RMA, and their cocrystals. (b) T_g of the NIC-RMA melt vs composition. Inset: DSC trace of a 1:2 liquid showing the glass transition. The T_g values of pure NIC and RMA cannot be determined owing to fast crystallization.

produce a glass, and its glass transition temperature T_g was measured on second heating. Figure 3b shows T_g as a function of melt composition. A curve is drawn through the data points and extrapolated to the limits of pure NIC and RMA to estimate their T_g values, which we could not measure directly owing to fast crystallization. The better glass-forming ability of NIC-RMA solutions over the pure liquids is reminiscent of the stabilization of metallic glasses by alloying. Table 4 summarizes key thermodynamic data.

Figure 4 shows the binary phase diagram of NIC and RMA. The raw data collected to construct this diagram (DSC scans of binary physical mixtures) are given in the Supporting Information. The diagram shows the melting of NIC and RMA (points 1 and 2), the congruent melting of NR Form 1 (3) and NR Form 2 (4), and the incongruent melting of N_4R (5) and NR_2 (6). The diagram shows three eutectic melting points: between NIC and NR Form 1 (7), between NR Form 1 and RMA (8), and between NIC and RMA (9). The incongruent melting of N_4R produces NIC crystals and a liquid phase, which was confirmed by hot-stage microscopy. The incongruent melting of NR_2 forms a liquid phase and NR Form 1 (or Form

Table 4. Thermal Properties of NIC-RMA Cocrystals

	T_m, °C	ΔH_m, J/g	ΔH_f, J/g[b]	ΔV_f, cm^3/kg[c]
RMA	131.7(0.1)	176.9(0.6)	0	0
NR_2	66.8(0.2)[a]	105.7(0.4)	−20(3)	2.3
NR Form 1	89.1(0.2)	140.8(0.4)	−23(3)	15.6
NR Form 2	85.2(0.2)	128.4(1.9)	−18(3)	25.3
N_4R	98.3(0.2)[a]	157.5(1.9)	−8(3)	28.0
NIC	128.3(0.1)	197.0(0.6)	0	0

[a]Incongruent melting. [b]ΔH_f is evaluated at 20 °C. [c]ΔV_f evaluated at 100 K but expected to be insensitive to T. The error in ΔV_f *is* estimated to be 2 cm^3/kg.

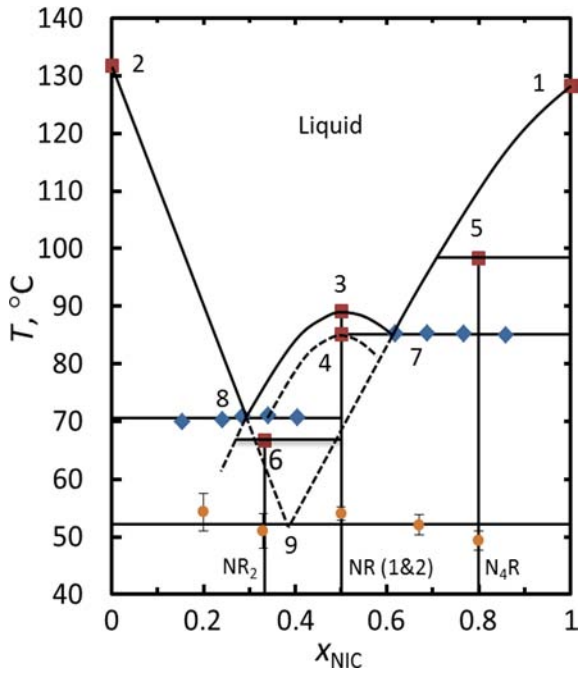

Figure 4. Binary phase diagram of NIC and RMA. The vertical lines at x_{NIC} = 0.33, 0.5, and 0.8 correspond to the cocrystals.

2), which is consistent with observations by hot-stage microscopy and Raman spectroscopy. There may be additional eutectic points in the phase diagram involving NR Form 2, whose liquidus curve is shown with a maximum at point 4, but they are not shown for clarity. Curve 1−7−9 is the phase boundary for NIC crystals in equilibrium with a NIC-RMA solution; curve 2−8−9 is the corresponding boundary for RMA crystals. Note that these curves are much steeper than predicted on the assumption of ideal mixing in the liquid state: the prediction would have the two curves crossing at ca. 95 °C and x_{NIC} = 0.55, rather than the observed 52 °C and x_{NIC} = 0.4 (point 9). Such deviation is expected for mixing NIC and RMA, a weak base and a weak acid.

Figure 5 illustrates the determination of the formation enthalpies ΔH_f of NIC-RMA cocrystals and the mixing enthalpies ΔH_{mix} of NIC and RMA in the liquid state.[10] To obtain ΔH_f, we integrate the heat-flow data of a cocrystal and the corresponding physical mixture of the component crystals (Figure 5a) from a common liquid-state temperature (140 °C) down to a common solid-state temperature (30 °C). The enthalpy of the cocrystal relative to the physical mixture is its formation enthalpy (ΔH_f in Figure 5b). Similarly, to obtain ΔH_{mix}, we integrate the melting endotherms of crystalline NIC, crystalline RMA, and their physical mixture from a common solid-state temperature (20 °C) to a common liquid-state

dx.doi.org/10.1021/ja4103887 | J. Am. Chem. Soc. 2013, 135, 18981−18989

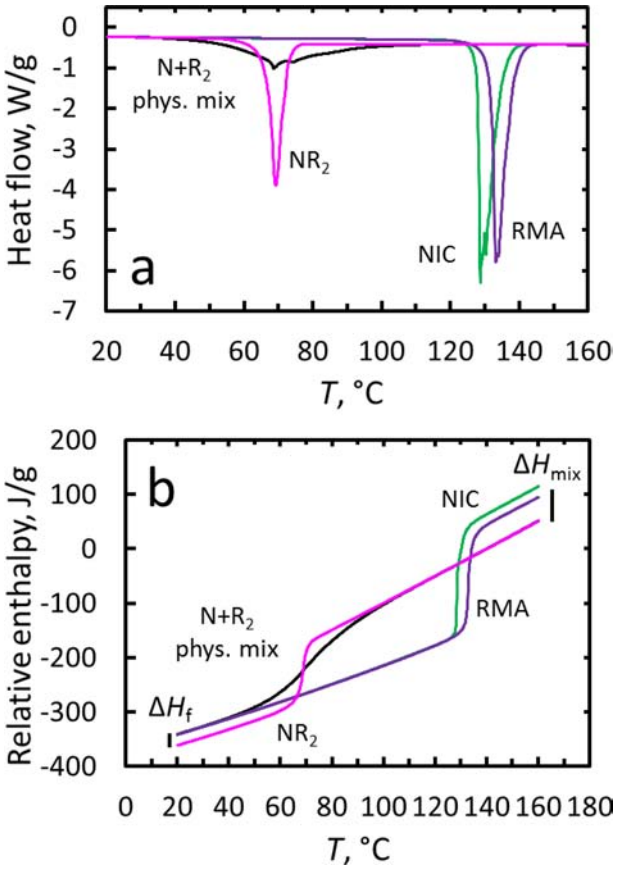

Figure 5. (a) DSC melting endotherms of NR_2, NIC, RMA, and a physical mixture of NIC and RMA at 1:2 molar ratio. (b) Relative enthalpies between NR_2, NIC, and RMA and the N + R_2 physical mixture. ΔH_f is the formation enthalpy of NR_2. ΔH_{mix} is the mixing enthalpy of NIC and RMA in the liquid state.

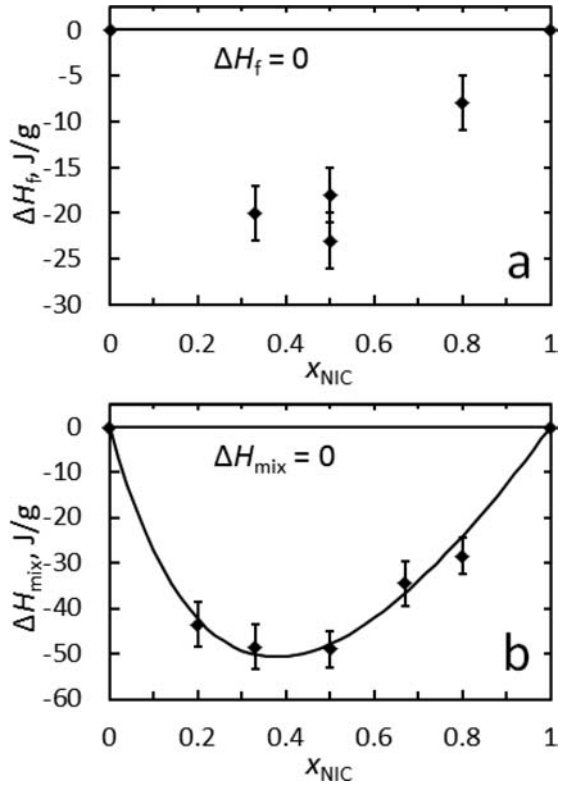

Figure 6. Formation enthalpies of NIC-RMA cocrystals and the mixing enthalpies of NIC and RMA liquids. Table 4 gives the values of ΔH_f. ΔH_{mix} = −28(4), −34(5), −49(4), −48(5), and −44(5) J/g for mixing liquid NIC and RMA at 4:1, 2:1, 1:1, 1:2, and 1:4 molar ratios (T = 160 °C).

temperature (160 °C). Assuming the enthalpy of mixing is negligible in the crystalline state, ΔH_{mix} is obtained from the enthalpy of the solution relative to the pure liquids (Figure 5b). Note that ΔH_f and ΔH_{mix} are evaluated at different temperatures (30 and 160 °C).

Figure 6 compares the ΔH_f and ΔH_{mix} data for the NIC-RMA system. In this comparison, note that ΔH_f is the enthalpy change for the solid-state reaction in eq 1 and ΔH_{mix} is the enthalpy change for the corresponding liquid-state reaction. For this system, ΔH_f and ΔH_{mix} are both negative (reactions are exothermic), indicating the mixed state has lower energy than the separated state. The larger ΔH_f in the solid state approximately correlates with a larger ΔH_{mix} in the liquid state. These negative enthalpy changes are expected for mixing a base (NIC) and an acid (RMA). The exothermic mixing of NIC and RMA is also consistent with their solution having a higher T_g than the pure liquids (Figure 3b): both phenomena indicate stronger intermolecular interactions in the mixed state.

The key finding of this work is that the formation of NIC-RMA cocrystals from their components (eq 1) lowers energy (ΔH_f < 0) but expands volume (ΔV_f > 0). This conclusion is supported by observations on a large number of cocrystals: three stoichiometric ratios and two polymorphs for the 1:1 cocrystal. The energy decrease upon cocrystallization is expected for a base (NIC) reacting with an acid (RMA); indeed, the two components mix exothermically in the liquid state (ΔH_{mix} < 0; Figure 6b), as do other similar acids and bases.[23] The expansion of volume, however, is unexpected, given the observation that acid−base mixing in the liquid state reduces volume.[18] Our survey of the CSD (Table 3) found that this volume expansion is general for NIC to cocrystallize with another component (typically an acid). Assuming the NIC-RMA cocrystals exemplify the behaviors of all NIC cocrystals, we anticipate that the anti-correlation between energy and volume is general for the cocrystallization of NIC.

The formation of NIC-RMA cocrystals is remarkable in reference to other physical processes for which enthalpy and volume typically increase or decrease in concert (positive correlation). Figure 7 shows typical enthalpy-volume correlations in several physical processes: (1) heating organic solids at 1 bar, $\Delta H/(\Delta V/V) = C_p/\alpha_V \approx 50$ J/g/(1% expansion); (2) melting crystals, $\Delta H/(\Delta V/V) \approx 10$ J/g/(1%);[24] (3) mixing organic liquids, $\Delta H/(\Delta V/V) \approx 10$ J/g/(1%);[25] (4) forming racemic compounds from opposite enantiomorphs, $\Delta H \approx 20$ J/g[11] and $\Delta V/V \approx 2\%$;[12] (5) converting low-temperature to high-temperature polymorphs, $\Delta H \approx 20$ J/g and $\Delta V/V \approx 2\%$.[26,27] Note the greater scatter in the last two processes (both solid-state reactions), for which the shaded areas are drawn to reflect approximately the ranges in the original reports.[11,12,26] In contrast to the processes listed above, the cocrystallization of NIC and RMA exhibits a negative correlation between enthalpy and volume. Such a negative correlation, however, is in common with ice melting (ΔH = 335 J/g and $\Delta V/V$ = −8%) and water freezing.

The simplest explanation for the anomalous formation properties of NIC cocrystals is that their structures contain stronger hydrogen bonds and are not simultaneously optimized

dx.doi.org/10.1021/ja4103887 | J. Am. Chem. Soc. 2013, 135, 18981−18989

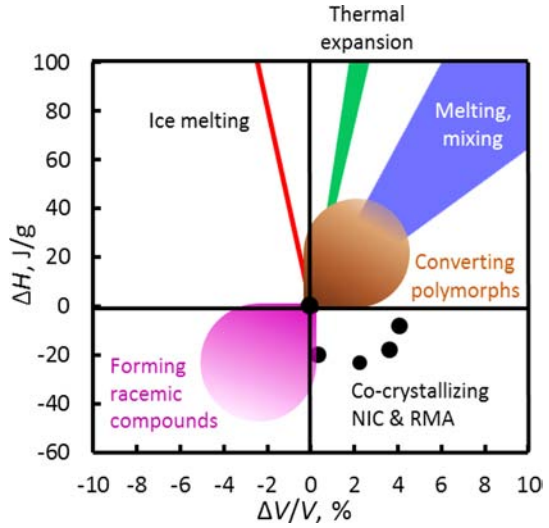

Figure 7. Enthalpy–volume correlation for the cocrystallization of NIC and RMA, in comparison with the typical relations for other physical processes. The cocrystallization reduces enthalpy but expands volume, in contrast to many other processes but analogous to water freezing.

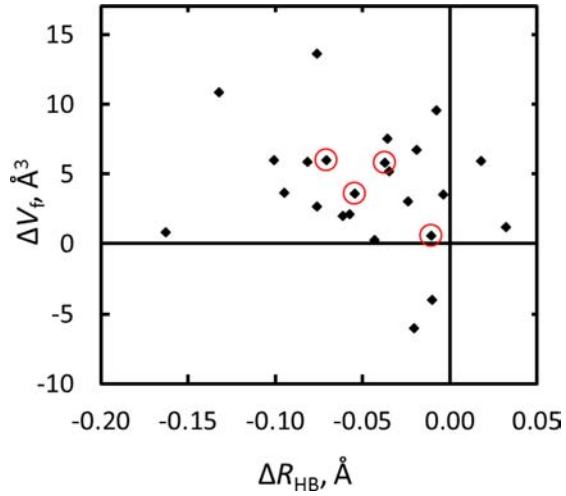

Figure 8. ΔV_f and ΔR_{HB} values of NIC cocrystals. The NIC-RMA cocrystals are circled: $\Delta R_{HB} = -0.054$ Å (NR Form 1), −0.037 Å (NR Form 2), −0.071 Å (N_4R), −0.010 Å (NR_2). As in ΔV_f calculations, R_{HB} of NIC at an unstudied temperature is extrapolated or interpolated from its values at 150 and 295 K. To calculate the ΔR_{HB} of NR Form 1 (JILZOU, solved at 150 K), the R_{HB} of RMA is taken to be the same as that at 100 K. For the other NIC cocrystals, ΔR_{HB} is calculated only if the coformer B crystal was solved at a temperature similar (within 5 K) to that of the cocrystal.

for efficient molecular packing. This interpretation is supported by the overall shortening of hydrogen bonds in NIC cocrystals relative to their components (Figure 8). To construct Figure 8, we calculate the change of hydrogen-bond length upon cocrystallization using an equation similar to eq 4:

$$\Delta R_{HB} = \langle R_{HB}\rangle_{cc} - \left[\frac{m}{m+n}\langle R_{HB}\rangle_A + \frac{n}{m+n}\langle R_{HB}\rangle_B\right] \quad (5)$$

where $\langle R_{HB}\rangle_{cc}$, $\langle R_{HB}\rangle_A$, and $\langle R_{HB}\rangle_B$ are respectively the average heavy-atom-to-heavy-atom distances for all hydrogen bonds in the cocrystal A_mB_n, component crystal A, and component crystal B. We use the program Mercury (version 3.1) to identify and measure hydrogen bonds and include only intermolecular hydrogen bonds. Figure 8 shows that the positive ΔV_f of NIC cocrystals correlates with a negative ΔR_{HB}, placing the data points mainly in the upper left quadrant. The data for NIC-RMA cocrystals (red circles) belong in the same population as the entire group. Given that shorter hydrogen bonds are generally stronger, we propose that NIC cocrystals contain stronger hydrogen bonds than their component crystals and speculate that, as a consequence of optimizing hydrogen bonding, the crystal structures fail to simultaneously achieve efficient molecular packing. The stronger hydrogen bonding is consistent with the cocrystallization of a weak acid and a weak base: on average, their hydrogen bonding should be stronger than that between the acid molecules or between the base molecules. This effect does not emerge in the formation of racemic compounds, because if one enantiomer is an acid, so is the opposite enantiomer.

In summary, the anomalous formation properties of NIC cocrystals ($\Delta H_f < 0$ and $\Delta V_f > 0$) may result from their stronger hydrogen bonding, which lowers energy but hinders efficient molecular packing. In this respect, the formation of NIC cocrystals is analogous to other processes with negative enthalpy–volume correlation, for example, the freezing of water and the transformation of β-resorcinol to α-resorcinol,[28] both processes lowering enthalpy, increasing volume, and forming stronger hydrogen bonds. It would be of interest to study other families of cocrystals (e.g., those of isonicotinamide) to test the generality of this idea.

CONCLUSION

This study has identified a remarkable system of cocrystals containing nicotinamide (NIC) and (*R*)-mandelic acid (RMA) in numerous stoichiometric ratios (4:1, 1:1 in two polymorphs, and 1:2) with anomalous formation properties. Single crystals were grown with seeds from melt crystallization and enabled the solution of their structures. The formation enthalpies of cocrystals were determined from their melting enthalpies and those of the physical mixtures of component crystals. The formation volumes of cocrystals were calculated from their specific volumes and those of the component crystals. We find that the formation of NIC-RMA cocrystals lowers energy, in agreement with the exothermic mixing of their liquids, but expands volume. This result is unexpected because most physical processes have positive enthalpy–volume correlations. A survey of the CSD found that all NIC cocrystals tend to have positive formation volumes (+3.9 $Å^3$/molecule or +17 cm^3/kg on average, corresponding to 2% volume expansion) and shorter hydrogen bonds. The NIC-RMA binary phase diagram was constructed that contains the congruent and incongruent melting of six crystalline phases.

These results are relevant for understanding the nature of cocrystallization and the prolific cocrystal former nicotinamide. As NIC cocrystallizes with another component (often a weak acid), the resulting structure may be optimized for stronger hydrogen bonding but fail to simultaneously achieve efficient molecular packing, in analogy with the freezing of water and the polymorphic transformation of resorcinol. NIC is one of the most prolific cocrystal formers, and this ability may reflect its proficiency to arrange itself, perhaps with conformational adjustment, to optimize hydrogen bonding while achieving adequately close packing. It would be of interest to extend the present study to other prolific cocrystal formers to test these ideas. Computational studies will be especially powerful for

dx.doi.org/10.1021/ja4103887 | J. Am. Chem. Soc. 2013, 135, 18981–18989

testing the anti-correlation between energy and volume in cocrystallization.

■ ASSOCIATED CONTENT

Supporting Information

Figures, tables, and CIF files giving melt crystallization of seed crystals and their XRD patterns, DSC data of binary physical mixtures, and crystallographic data of N_4R, NR_2, and RMA at 100 K. This material is available free of charge via the Internet at http://pubs.acs.org.

■ AUTHOR INFORMATION

Corresponding Author

lyu@pharmacy.wisc.edu

Notes

The authors declare no competing financial interest.

■ ACKNOWLEDGMENTS

We thank the National Institute for Pharmaceutical Technology and Education (NIPTE) and the National Science Foundation (DMR 1234320) for supporting this work. We thank Brian Dolinar and Dr. Ilia Guzei for structural solution and Dr. Joseph Krzyzaniak, Dr. Neil Feeder, and Prof. William Jones for helpful discussions.

■ REFERENCES

(1) Findlay, A.; Campbell, A. N.; Smith, N. O. *Phase Rule and Its Applications*; Dover: Mineola, NY, 1951.
(2) Childs, S. L.; Chyall, L. J.; Dunlap, J. T.; Smolenskaya, V. N.; Stahly, B. C.; Stahly, G. P. *J. Am. Chem. Soc.* **2004**, *126*, 13335−13342.
(3) Almarsson, Ö.; Zaworotko, M. J. *Chem. Commun.* **2004**, 1889−1896.
(4) McNamara, D. P.; Childs, S. L.; Giordano, J.; Iarriccio, A.; Cassidy, J.; Shet, M. S.; Mannion, R.; O'Donnell, E.; Park, A. *Pharm. Res.* **2006**, *23*, 1888−1897.
(5) Chattoraj, S.; Shi, L.; Sun, C. C. *CrystEngComm* **2010**, *12*, 2466−2472.
(6) Bolton, O.; Matzger, A. J. *Angew. Chem., Int. Ed.* **2011**, *50*, 8960−8963.
(7) Friščić, T.; Jones, W. *Faraday Discuss.* **2007**, *136*, 167−178.
(8) Lemmerer, A.; Esterhuysen, C.; Bernstein, J. *J. Pharm. Sci.* **2010**, *99*, 4054−4071.
(9) Berry, D. J.; Seaton, C. C.; Clegg, W.; Harrington, R. W.; Coles, S. J.; Horton, P. N.; Hursthouse, M. B.; Storey, R.; Jones, W.; Friščić, T.; Blagden, N. *Cryst. Growth Des.* **2008**, *8*, 1697−1712.
(10) Zhang, S.-W.; Guzei, I. A.; de Villiers, M. M.; Yu, L.; Krzyzaniak, J. F. *Cryst. Growth Des.* **2012**, *12*, 4090−4097.
(11) Jacques, J.; Collet, A.; Wilen, S. H. *Enantiomers, Racemates, and Resolutions*; Krieger: Malabar, FL, 1991.
(12) Brock, C. P.; Schweizer, W. B.; Dunitz, J. D. *J. Am. Chem. Soc.* **1991**, *113*, 9811−9820.
(13) Yu, L. *Acc. Chem. Res.* **2010**, *43*, 1257−1266.
(14) Li, J. J.; Bourne, S. A.; Caira, M. R. *Chem. Commun.* **2011**, *47*, 1530−1532.
(15) Chen, S.; Guzei, I. A.; Yu, L. *J. Am. Chem. Soc.* **2005**, *127*, 9881−9885.
(16) Miwa, Y.; Mizuno, T.; Tsuchida, K.; Taga, T.; Iwata, Y. *Acta Crystallogr., Sect. B* **1999**, *55*, 78−84.
(17) Patil, A. O.; Pennington, W. T.; Paul, I. C.; Curtin, D. Y.; Dykstra, C. E. *J. Am. Chem. Soc.* **1987**, *109*, 1529−1535.
(18) Handa, Y. P.; Benson, G. C. *Fluid Phase Equilib.* **1979**, *3*, 185−249.
(19) Bruno, I. J.; Cole, J. C.; Edgington, P. R.; Kessler, M.; Macrae, C. F.; McCabe, P.; Pearson, J.; Taylor, R. *Acta Crystallogr., Sect. B* **2002**, *58*, 389−397. The version used for this work is 5.34 (November 2012) with the Feb 2013 and May 2013 updates.
(20) van de Streek, J.; Motherwell, S. *CrystEngComm* **2007**, *9*, 55−64.
(21) Price, C. P.; Glick, G. D.; Matzger, A. J. *Angew. Chem., Int. Ed.* **2006**, *45*, 2062−2066.
(22) Gunn, E. M.; Guzei, I. A.; Yu, L. *Cryst. Growth Des.* **2011**, *11*, 3979−3984.
(23) Nandi, A. K.; Bhattacharyya, S. N. *J. Chem. Eng. Data* **1993**, *38*, 358−360.
(24) Al-Mahdi, A. A. K.; Ubbelohde, A. R. *Proc. R. Soc. A* **1953**, *220*, 143−156.
(25) Hansen, A. R.; Eckert, C. A. *Fluid Phase Equilib.* **1990**, *60*, 59−80.
(26) Gavezzotti, A.; Fillippini, G. *J. Am. Chem. Soc.* **1995**, *117*, 12299−12305.
(27) Burger, A.; Ramberger, R. *Mikrochim. Acta* **1979**, *2*, 259−271.
(28) Monteath Robertson, J.; Ubbelohde, A. R. *Proc. R. Soc. A* **1938**, *167*, 122−135; **1938**, *167*, 136−147.